ORIGINAL PAPER

Effect of mechanical milling induced strain and particle size reduction on some physical properties of polycrystalline yttrium iron garnet

K B Modi[1]*, S N Dolia[2] and P U Sharma[3]

[1]Department of Physics, Saurashtra University, Rajkot 360 005, India

[2]Department of Physics, University of Rajasthan, Jaipur 302 055, India

[3]M. N. College, Visnagar 384 315, India

Abstract: The effect of mechanical milling induced strain and particle size reduction on structural, micro-structural and magnetic properties of un-milled and milled polycrystalline samples of yttrium iron garnet, $Y_3Fe_5O_{12}$ (YIG), for different duration, 3, 6, 9 and 12 h, have been studied using X-ray powder diffractometry, scanning electron microscopy, infrared spectroscopy, Mossbauer spectroscopy, high field magnetization and low field (0.5 Oe) ac susceptibility measurements. YIG on milling is found to decompose into $Y_3Fe_5O_{12}$ and yttrium ortho-ferrite, $YFeO_3$, phases, as reflected from various characterizations. The infrared and Mossbauer spectroscopic studies give an indication for the loss of oxygen on milling. The shift in Neel temperature with particle size reduction has been described by finite size scaling. The observed changes in M–H loop are mainly due to strain induced increase in surface anisotropy on milling. The two transitions have been observed in the thermal variation of ac susceptibility curves, corresponding to ferrimagnetic YIG-phase and another due to weak ferromagnetic $YFeO_3$-phase.

1. Introduction

Yttrium iron garnet, $Y_3Fe_5O_{12}$ (YIG), is a widely investigated compound owing to its specific magneto-optical properties [1], e.g. in electromagnetic transmitters with YIG-based magnetic feeders used for seabed logging application [2]. Three-dimensional magneto photonic crystals composed of $Y_3Fe_5O_{12}$ and $BiFeO_3$ possess interesting optical and magneto-optical properties [3]. $Y_3Fe_5O_{12}$ in single crystalline, polycrystalline, thin film and nanoparticles forms, finds applications in magnetic microwave devices, absorber or shielding materials, irradiation studies etc. [4, 5]. Recently, a significant magneto dielectric coupling has been reported in $Tb_3Fe_5O_{12}$ and $Lu_3Fe_5O_{12}$ garnets, showing the potential for new applications. In this class of materials, $Y_3Fe_5O_{12}$ is the most studied and serves as a role model in many applications.

However, high sintering temperature (>1,450 °C) and long soaking time (>10 h) are required to synthesize YIG materials with sufficiently high density [6]. Furthermore, based on the atomistic simulation studies, it has been suggested that in yttrium iron garnet, formation of perovskite $YFeO_3$ phase rather than non-stoichiometric phases, is more likely on the application of an external agencies (swift heavy ion irradiation, high energy ball milling, large size cationic substitution, etc.), as there is very little difference in the lattice energy of the two phases: $Y_3Fe_5O_{12}$ and $YFeO_3$ [7].

Due to their reduced size, these nano particles may possess novel and/or improved properties in comparison to the bulk materials. This has renewed interest to study different properties of pure and substituted magnetic oxide systems, in general and ferrites, in particular in the

*Corresponding author, E-mail: kunalbmodi2003@yahoo.com

nanocrystalline regime. Various synthesis techniques have been used for preparation of nano materials. Mechanical attrition—ball milling is a technique which has also been used widely for preparation of nano structured materials [8]. Because of its simplicity and the applicability to essentially all classes of materials, this has become a popular method to make nanocrystalline materials [9, 10]. The major advantage often quoted about the ball milling technique, is the possibility for easily scaling up to tonnage quantities of materials for various applications. In fact contamination problem is often given as a reason to dismiss the method at least for some materials [11]. Earlier, the effectiveness of a milling process has been assessed considering changes in the particle size, its distribution and shape. But recently, it has been apparent that in order to characterize a powder more fully, the strain induced during the milling process has to be considered.

In the last couple of years many research articles describing the effect of grain size on various properties of pure yttrium iron garnet synthesized by various soft chemical routes (bottom-up approach) are available in the literature [12–18]. Concentrating only on nanoparticles prepared by high energy ball milling (top-down approach) and its effect on various physical properties of pure iron garnets, only a couple of research reports are available [19–24]. Interest in nano structured materials based on yttrium iron garnet is explained by both the fundamental problems of the physics of nanocrystalline magnetic materials and the prospects of their use in coatings, nano composites, ferro-fluids, etc. [13]. The majority of previous investigations have focused on its magnetic and magneto-optical properties. There have been a few studies on the dielectric properties of YIG [25, 26].

In this connection, we have studied earlier the elastic properties determined from ultrasonic pulse transmission technique [27], Mossbauer spectroscopic studies [28] on $Y_{3-x}Fe_{5+x}O_{12}$ system and pre and post effect of swift heavy ion irradiation (SHII) on M–H loop characteristics [29], SHII induced ion beam mixing employing X-ray diffraction and Mossbauer spectroscopy [30], dielectric properties [31], structural and electrical properties [32] and permeability spectral analysis and microstructural parameter determination [33], for yttrium—excess polycrystalline yttrium iron garnet, $Y_{3+x}Fe_{5-x}O_{12}$ ($x = 0.0$–0.6), system. On the other hand, the effect of high energy mechanical milling on the structural properties [34], X-ray Debye temperature [35], infrared spectral evolution, elastic, optical and thermodynamic properties [36] of $Ni_{0.5}Zn_{0.5}Fe_2O_4$ spinel ferrite composition have been investigated.

This paper is devoted to study the effect of high energy mechanical milling on structural, micro-structural, optical and magnetic properties of $Y_3Fe_5O_{12}$ as a function of particle size, milling time and temperature. This comprehensive study contributes new dimension in the field of nanocrystalline ferrite materials and structure—property co-relation. Detailed review articles on the mechanical alloying and milling, properties and applications of yttrium iron garnet can be found in [37, 38].

2. Experimental details

Bulk quantity (about 15 g) of polycrystalline yttrium iron garnet, $Y_3Fe_5O_{12}$ (YIG), composition was prepared by the usual double sintering ceramic technique. 99.9 % pure powders of ferric oxide, Fe_2O_3 and yttrium oxide, Y_2O_3, supplied by E. Merck were thoroughly mixed in appropriate stoichiometry to yield the desired composition and then wet-ground by blending with acetone in an agate mortar and pestle for 4 h. The mixture was dried and pressed into pellets at a pressure of 2×10^7 kg/m^2 using a Hydraulic Press (BIMPEX Machines Instrumentation, Mumbai, India).

The pellets were pre-sintered at 1,100 °C for 24 h. After regrinding and re-pelletizing, in the final sintering process, the sample was kept at 1,500 °C for 24 h and slowly cooled to room temperature at the rate of 2 °C/min. The pre-sintering and sintering processes were carried out under an air atmosphere. The synthesized sample (un-milled sample) was milled in an Ar-atmosphere up to 12 h using a high energy laboratory ball milling (SPEX 8000 mixer). Silicon balls were used for ball milling in agate vial. To improve particle mobility during milling process, water was added to the container. The milling process was interrupted after selected milling duration (3, 6, 9 and 12 h) to remove small amount of powder, which was heated in air at 50 °C to completely dry.

The experimental details regarding the X-ray powder diffractometry, infrared spectroscopy, scanning/transmission electron microscopy and 57 Fe Mossbauer spectroscopic measurements had been described elsewhere [27, 28, 34, 36]. The ac susceptibility measurements on powdered samples were made in the temperature range 300–850 K using a double coil set-up [39] operating at a frequency of 263 Hz with r.m.s. field of 40 A/m. To investigate the macroscopic magnetic behaviour, magnetic moments of the samples at 20 K were recorded using a vibrating sample magneto meter (VSM) going up to 9 kOe of an external magnetic field.

3. Results and discussion

3.1. X-ray powder diffraction patterns analysis

The X-ray powder diffraction (XRD) patterns recorded at 300 K for un-milled and milled samples of $Y_3Fe_5O_{12}$ for 3,
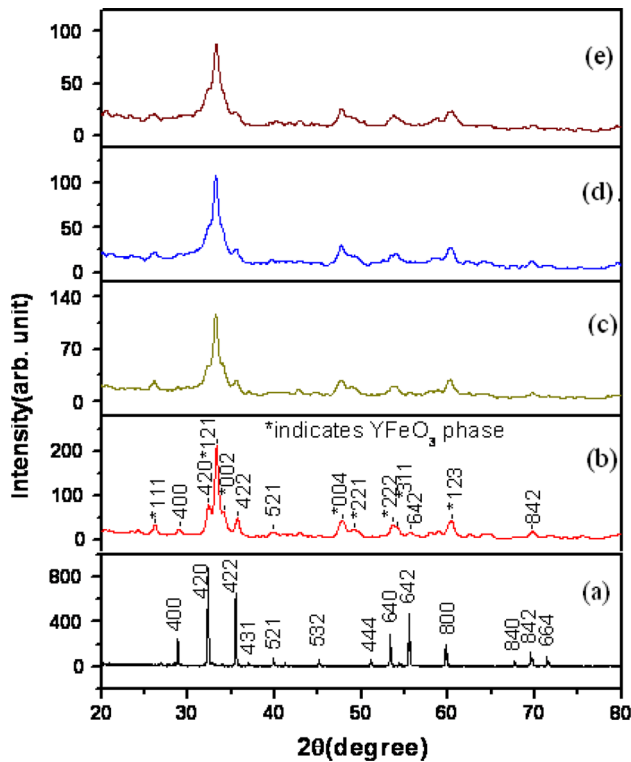
Fig. 1 X-ray diffraction patterns for (**a**) un-milled (**b**) 3 h (**c**) 6 h (**d**) 9 h and (**e**) 12 h milled samples of YIG

6, 9 and 12 h are shown in Fig. 1(a)–1(e). Refinement analysis leading to indexing and calculation of the structural parameters is performed using the powder–x software [40]. The patterns confirm the formation of single phase *bcc* garnet structure for un-milled sample, with no extra lines corresponding to any other crystallographic phase or un-reacted ingredient. It is found from the patterns that the additional orthorhombic phase of yttrium orthoferrite (YFeO$_3$) (marked as *) grows in intensity for the milled samples.

The XRD patterns for all the milled samples are indexed for *bcc*-garnet phase (space group: O_h^{10}-*Ia3d*) and orthorhombic phase of YFeO$_3$ (space group: *Pnma*) using standard structural data files obtained from PCPDFWIN

program (PDF card No: 83-1027 and 86-0171, respectively) and the corresponding Bragg planes are shown in the profiles. The values of lattice constants, determined for both the phases for all the samples using X-ray data, are shown in Table 1 for different milling times.

It is observed that the lattice constants for orthorhombic phase remain uninfluenced by milling time and have values close to that of pure yttrium orthoferrite [41]: (a = 5.562 Å, b = 7.577 Å and c = 5.257 Å). On the other hand, lattice constant value for garnet phase increases linearly with the increase in milling time up to 6 h and then decreases with further increase of milling time (Table 1).

The observed increase in lattice constant for garnet phase from un-milled sample to 6 h milled samples could be due to one or more of the following causes: (i) The strong internal strain introduced during mechanical milling treatment causing increase in plane spacing results in the unit cell expansion. (ii) The formation and presence of Fe^{2+} ion with larger cationic radius of 0.74 Å, as compared to 0.64 Å of Fe^{3+} ions, may also be the reason for lattice expansion. The formation of ferrous ion is quite probable in such systems. (iii) There could be un-paired electronic orbital at the outer surface dipoles repelling each other and resulting in a larger value of equilibrium lattice constant than in the bulk crystal [42]. (iv) The observed increase in unit cell parameter may be due to a negative pressure effect [8], which is associated with decreasing grain size in this oxide system.

The second probability is ruled out as presence of Fe^{2+} is reflected clearly in isomer shift value in Mössbauer spectral analysis, as ferrous ions have larger positive isomer shifts than ferric ions. According to Drickamer et al. [43], transition metal oxides possess partial covalence due to the interaction between the 3*d* electrons of the transition metal and the oxygen nucleus. This covalence is found to increase with increasing pressure. The negative pressure effect increases the ionicity, breaking the directional nature of the bonds and hence stabilizing the more symmetrical structure. For example, Ayyub et al. [42] have observed the transformation of rhombohedral structure of α-Fe$_2$O$_3$ to the

Table 1 Percentage (%) of phase, lattice constants, bulk density (ρ) and X-ray density (ρ_x) values for un-milled and milled samples of YIG

Sample	% of phase		Lattice constants ± 0.002 Å				Bulk density (ρ) (g/cm^3)	X-ray density (ρ_x) (g/cm^3)
Y$_3$Fe$_5$O$_{12}$	YIG	YFeO$_3$	YIG	YFeO$_3$				
			a = b = c	a	b	c		
Un-milled	100	–	12.377	–	–	–	4.572	5.170
3 h	25.6	74.4	12.382	5.26	7.59	5.55	4.890	5.164
6 h	21.1	78.9	12.435	5.25	7.57	5.58	4.586	5.098
9 h	25.2	74.8	12.380	5.25	7.57	5.58	4.545	5.166
12 h	26.9	73.1	12.371	5.25	7.58	5.58	4.527	5.177

more symmetrical cubic structured gamma-Fe_2O_3 on decreasing grain size. Similarly, Prabhu et al. [8] have found that on decreasing grain size by mechanical milling in the case of copper ferrite, $CuFe_2O_4$, tetragonal distortion or deviation from cubic symmetry ($c/a > 1$) decreases and the system transfers to the more symmetrical cubic structure ($c/a = 1$). In the present case un-milled yttrium iron garnet with more symmetrical single bcc-garnet phase transforms into the less stable mixed phase system on milling (Table 1). Thus, the fourth probability is also ruled out. Hence, the first and third causes may be responsible for the observed increase in lattice constant value for 3 and 6 h milled samples.

The probable reasons for reduction in lattice parameter for 9 and 12 h milled samples could be the followings: (i) the high energy ball milling process, known to induce cation redistribution in spinel ferrites and garnets [44]; (ii) presence of lattice defects and their influence on the nanoparticles, especially on the surface. In nano particles; surface area and surface tension of the particles are high. This in turn results in a tendency to shrink the lattice causing reduction in the lattice constant [44]. (iii) Some of the yttrium ions diffuse to the grain boundaries reacting with Fe to form $YFeO_3$. The lattice may be compressed by the inter-granular secondary phase due to the difference in the thermal expansion coefficients [45].

The percentage formation of the bcc garnet phase and the yttrium orthoferrite, $YFeO_3$ phase for these samples is determined taking intensity ratios of most intense peak of both the phases using the method described elsewhere [46]. The percentage of orthoferrite phase is: $(100 \times I_{ortho})/(I_{ortho} + I_{garnet})$, where I_{ortho} and I_{garnet}, are the integrated highest band intensities of orthoferrite and garnet phase X-ray diffraction peaks, respectively. Accordingly, the calculated percentage of orthoferrite phase is ~ 75 %. The maximum percentage of $YFeO_3$ formation is found for 6 h milled sample (Table 1). The variation of bulk density (ρ) and X-ray density (ρ_x) of $Y_3Fe_5O_{12}$ composition as a function of milling time is given in Table 1. The variation of ρ_x is consistent with the change in lattice constant (a) as a function of milling duration (Table 1).

3.2. Particle size, strain, surface area and surface energy determination

The average particle size (D) for the ball milled samples is calculated from the broadening of the respective high intensity (420) peak for YIG phase and (121) peak for $YFeO_3$ phase using the Debye–Scherrer formula: $D = (K\lambda)/(B \cos \theta)$. Here, λ is the wavelength of the CuK_α radiation (1.54059 Å), shape factor $K = 0.9$, related both to the crystalline shape and the way in which B and D are defined. B is the contribution to the XRD peak width (FWHM) due

to the small size of crystallites in radians. The contribution must separate out from the measured line width B_m, which includes instrumental broadening, B_{ins}, is always present irrespective of the particle size. For this, one can record XRD pattern of a well crystallized, bulk standard material such as silicon powder under identical geometrical conditions and measure the peak width, B_{ins}. Usually, instrumental broadening (B_{ins}) of a conventional X-ray powder diffractometer is $0.1°$. The broadening parameter B is obtained from the relation: $B = (B_m^2 - B_{ins}^2)^{1/2}$, where, $B_{ins} = 0.1°$ (= 0.00174 radian).

Here, the particle size is calculated for both the phases, considering the B (FWHM) obtained by Gaussian fitting of most intense peak of both the phases. The average particle size reduces from ~ 26 nm for 3 h milled sample to ~ 10 nm for 12 h milled sample (Table 2). The particle size decreases with increasing milling time because the kinetic energy generated by the series of collisions among balls is transformed to the system.

The particle size when calculated at different Bragg's angle (θ) values is at variance, indicating the presence of strain. Along with reduction in particle size, creation of non-uniform strain in the system also contributes in peak broadening, which is due to systematic shift of atoms from ideal positions, creation of point defects, plastic deformation or poor crystallization produced in the system as a result of prolonged high energy ball milling. Therefore, we have calculated strain (non-uniform) produced in the system as a result of milling. The probability of uniform strain is ruled out based on the fact that uniform strain contributes to shifting of d-spacing of the planes and hence the change in lattice constant values, but change in d-spacing values of only YIG phase peaks and not in the $YFeO_3$ phase peaks is observed. It is found that the diffraction lines corresponding to garnet phase shift to lower Bragg angle for 3 and 6 h milled samples, while it shifts to higher angle for 9 and 12 h milled samples with reference to peak positions for un-milled sample. The reduction in diffraction line intensity has also been observed in Fig. 1(b)–1(e). These observations suggest that non-uniform strain is produced in the samples due to mechanical milling.

The average lattice strain of all the milled samples has been calculated using the formula given by Stokes and Wilson [47] who first observed that strained or imperfect crystals contain line broadening of a different sort, from the broadening that arises from small crystallite size. Accordingly, lattice strain value can be calculated from the relation [48]: $\varepsilon_{str} = \beta_i/\{4 \tan\theta\}$, where, ε_{str} is the weighted average strain and β_i is the integral breadth of a reflection located at 2θ (in radians). As milling time increases, value of lattice strain increases (Table 2).

Attempt has been made to calculate surface area (S) and equivalent surface free energy for all the milled samples.

Table 2 Particle size, lattice strain, surface area (S) and equivalent surface free energy values for un-milled and milled samples of YIG

Sample $Y_3Fe_5O_{12}$	Particle size (nm)			Lattice strain (%)			Surface area (S) blank;(cm^2/g) $\times$ 10^4	Equivalent surface free energy (cal/g)
	YIG	YFeO$_3$	Average	YIG	YFeO$_3$	Average		
Un-milled	1.8 (µm)	–	–	–	–	–	–	–
3 h	24.8	26.2	25.5	–	–	–	48.11	11.4
6 h	16.2	15.6	15.9	0.981	0.732	0.856	82.29	19.5
9 h	13.2	13.4	13.3	0.910	0.910	0.910	99.27	23.5
12 h	9.4	11.4	10.4	1.083	1.042	1.062	127.44	30.2

Assuming all the particles to be spherical, the specific surface area in metre square per gram is given by [48]: $S = 6,000/D \rho$, where D is the particle diameter in nm and ρ is the density of the particle in g/cm^3. The specific surface area (Table 2) of the particle increases as the particle size decreases.

The surface free energy calculated assuming the particles to be spheres with a surface energy of 1,000 erg/cm^2 [49], increases with decreasing particle size (Table 2). In the case of nanoparticles, surface atoms are not bounded to the maximum number of nearest neighbours and are therefore in a higher energy state than the atoms at interior positions. The bonds of these surface atoms that are not satisfied give rise to a surface energy. In the field of nano-magnetism this surface energy plays a very crucial role. The surface area and equivalent surface free energy for all the samples are given in Table 2.

3.3. Infrared spectral analysis

Room temperature (300 K) infrared spectra in the wave number range 400–1,000 cm^{-1} for the different samples are shown in Fig. 2(a)–2(d). No absorption band is observed above 700 cm^{-1}. The spectrum of un-milled sample exhibits three bands at 572.76, 601.69, 663.40 cm^{-1} and can be assigned to asymmetric stretching of the tetrahedron in the YIG [6]. There are characteristic bands of the garnets [50]. FT-IR spectra of 3, 6 and 12 h milled samples are characterized by absorption bands at 569 ± 5 and 456 ± 7 cm^{-1}.

It has been reported by Mathur et al. [51] that these two absorption bands correspond to the Y–O and Fe–O stretching frequencies of YFeO$_3$ compound. On the contrary, it has been well establish by Venugopalan et al. [52], that the absorption bands associated with the heavier Y^{3+} ions (88.9 amu) lay in the region below 300 cm^{-1}. On the other hand, based on infrared and electronic spectral studies of rare earth perovskites [51] it has been shown that IR spectra of LnAO$_3$ (Ln is the rare earth ion or yttrium and
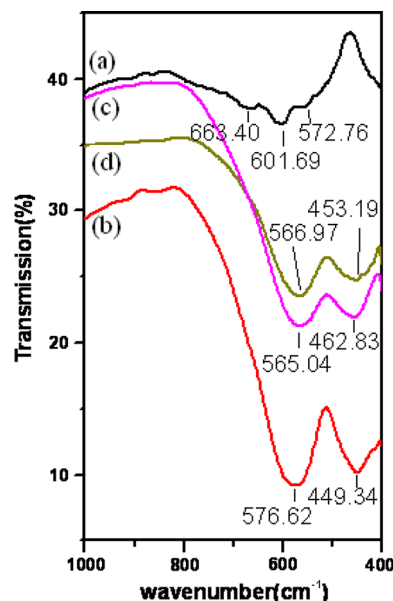

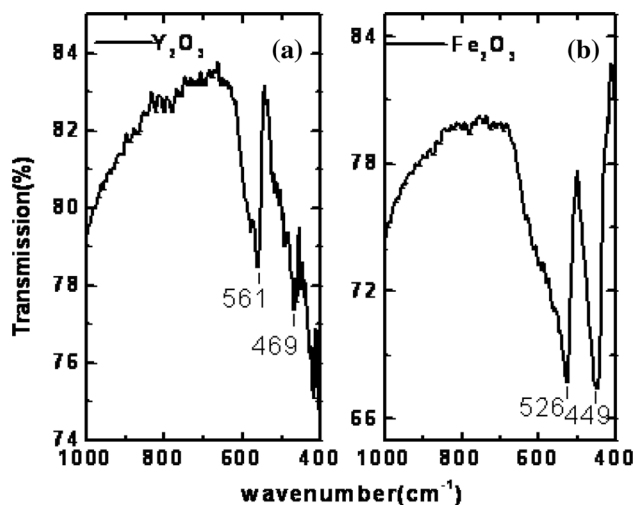**Fig. 2** Room temperature (300 K) infrared spectra for (**a**) un-milled (**b**) 3 h (**c**) 6 h and (**d**) 12 h milled samples of YIG

Fig. 3 Infrared spectra of (**a**) Y$_2$O$_3$ and (**b**) Fe$_2$O$_3$ at 300 K

A=Cr, Mn or Fe) perovskites are comparable to the spectra of the corresponding transition metal sesquioxides, A_2O_3. This implies that Ln ion does not affect IR spectra of perovskites compounds. Also recorded IR spectra of constituent oxides: Y_2O_3 and Fe_2O_3, are shown in Fig. 3(a) and 3(b), respectively.

The spectra show identical nature with two absorption bands in wave number range studied. These spectra are also identical in nature with those observed for milled samples of YIG. In the present case, the milled samples possess mixed phase of bcc garnet phase and orthorhombic phase of $YFeO_3$. Based on the above facts, it is clear that the two absorption bands observed for Y_2O_3 or milled samples of YIG cannot be due to Y–O vibrations.

It is concluded that high frequency absorption band at 569 ± 5 cm^{-1} is due to combine effect of asymmetric stretching vibrations of the tetrahedron of the YIG-phase and the motion of the in-plane oxygen atoms of $YFeO_3$-phase. The low frequency absorption band at 456 ± 7 cm^{-1} involves bending motion of the tetrahedral of YIG-phase, which is not observed for the un-milled sample of YIG but may be enhanced due to mechanical milling induced strain in the milled samples, as well as the apical oxygen vibrations of $YFeO_3$-phase. These results are consistent with IR/Raman spectral analysis of materials with similar structure [52, 53].

A careful examination of IR spectra of milled samples show that (i) high frequency absorption band shifts towards lower frequency side, (ii) low frequency band shifts towards higher frequency side on milling and (iii) intensity of absorption bands for 3 h milled sample is maximum while for 6 and 12 h milled samples intensity remains unaffected by milling time. Intensity of absorption bands for 12 h milled sample is slightly greater than absorption bands intensity for 6 h milled sample.

The observed shifting of the bands may be due to microstructural changes. The Fe–O bond lengths and angles show a variation because of the mechanical milling induced strain. The observed change in position of absorption bands with milling time may also be due to oxygen vacancies [54, 55] created by high energy ball milling. On the other hand, it is known that intensity of infrared absorption bands can give useful information concerning the change of electric dipole moment with inter-atomic distances and the charge on each ion. Based on the above fact it is felt that for 3 h milled sample, relative displacement of atoms (d_i) and the effective charge on different ions (q_i) get changed in a such a way that the magnitude of electric dipole moment ($p_i = q_i \cdot d_i$) increases and as a result intensity of the absorption band. The observed change in intensity of absorption bands for 6 and 12 h milled samples may be explained in a similar way. For a thorough understanding infrared reflectivity

measurements and the Rietveld refinement of X-ray data may be useful.

3.4. Scanning electron microscopy (SEM) and transmission electron microscopy (TEM)

The scanning electron micrographs of un-milled and milled samples of YIG are shown in Fig. 4(a)–4(d). It is observed that the milling of YIG material markedly enhances densification of the material. The average particle size can be estimated as 1.8 μm for the un-milled sample. It is also observed that the particles are stuck to each other in a regular and uniform manner to form a network-like structure. It is evident that morphology of the milled samples deviate from the un-milled sample: 3 and 6 h milled samples have particles with sizes that vary over a wide range and the small particles are getting agglomerated due to generated heat during the milling process. The 12 h milled sample shows multi-layer type grain growth.

Figure 5(a) and 5(b) shows typical TEM micrographs of 3 and 6 h milled samples of $Y_3Fe_5O_{12}$, respectively. It is seen that the particles are quite well dispersed and are fairly uniform in size. The particle size decreases with increasing milling time. Apart from that, the particle size distribution is quite narrow. From the micrographs it is observed that the milled samples show nearly spherical shape particles which may be because of the reduced size of the particles.

The particle size and its distribution is one of the most basic parameter in nanoparticles research. The X-ray diffraction pattern analysis gives the average crystallite size and no clue about its distribution. On the other hand, TEM can be used to measure the particle size of individual particles and quantify the particle size distribution in the sample. Normally, the particle size estimated from TEM is slightly greater than the particle size estimated from X-ray diffraction pattern analysis using Scherrer's formula, because X-ray diffraction gives information of the crystalline region only and the contribution from the amorphous grain surface does not contribute. On the other hand, TEM gives the complete picture of the nano-particles [56].

3.5. ^{57}Fe Mössbauer spectroscopic study

Figure 6(a)–6(d) shows the Mössbauer spectra of un-milled and milled (3, 6 and 12 h) samples of YIG at 300 K. The dots represent the experimental data and the continuous curve results from the least square fitting of the experimental data with the Lorentzian function. The ratio of the intensities of the peaks in a sextet has been fixed as 3:2:1::1:2:3 assuming random orientation of grains in polycrystalline samples. The relative intensities of the Mössbauer spectra of octahedral and tetrahedral sites of YIG are fixed to the ratio of their site population as 2:3.
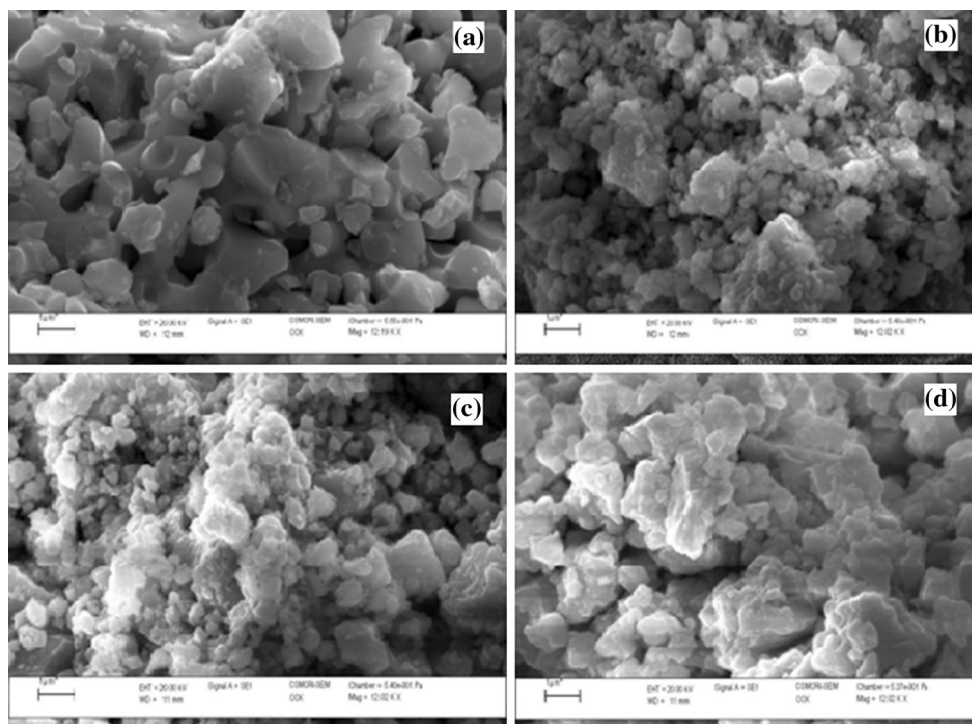
Fig. 4 SEM images for (**a**) un-milled (**b**) 3 h (**c**) 6 h and (**d**) 12 h milled samples of YIG
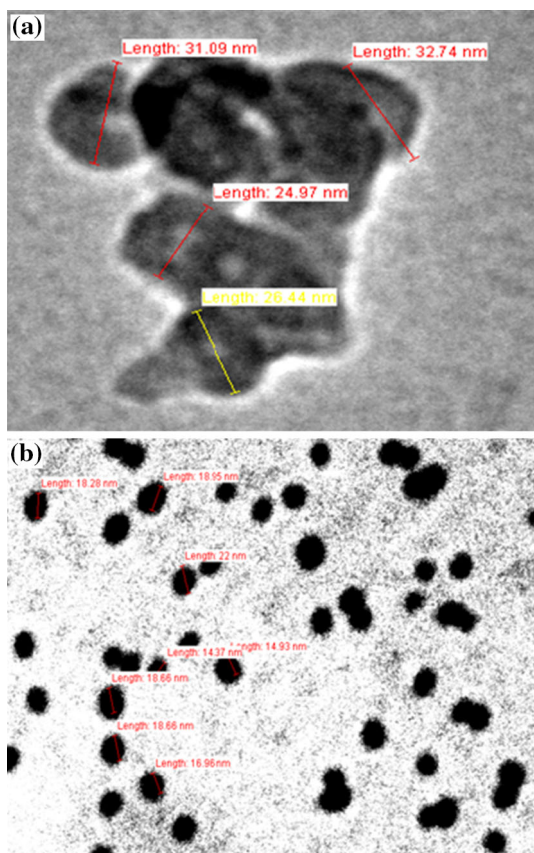

Fig. 5 TEM images for (**a**) 3 h and (**b**) 6 h milled samples of YIG

The Mössbauer spectrum for un-milled sample exhibits two superimposed asymmetric Zeeman split sextets, one due to Fe^{3+} ions at the tetrahedral (d-) and other due to the Fe^{3+} ions at the octahedral (a-) sites of the garnet structure. The peak area ratio of the d- to a-sites, $\Delta d/\Delta a$, is ≈ 1.5, which is typical value for YIG [57]. The magnetic hyperfine fields are 490 and 397 kOe for the a- and d-sites, respectively and are in agreement with earlier reports [58, 59]. The Zeeman lines for the d-sites are broader than those for the a-sites, which suggest distribution of magnetic hyperfine fields resulting from a perturbation in the sublattice [29].

In order to gain more information regarding the complicated phase evolution of YIG during milling, Mössbauer measurements have been carried out for the samples with various milling duration. On milling, un-milled sample of YIG for 3 h, a super-paramagnetic singlet and for 6 and 12 h milled samples, a super-paramagnetic doublet with a large line-width are obtained along with sextets arising from YIG and yttrium orthoferrite ($YFeO_3$) phases. The tetrahedral site environment of garnet phase is disturbed in such a way that it is not resolved in Mossbauer spectra of the milled samples. It has been reported that when YIG is subjected to swift heavy ion irradiation, the tetrahedral sites are preferentially destroyed with respect to the octahedral ones [60, 61]. In the present case, it is conjectured that similar type of mechanism is taking place by high energy ball-milling that has destroyed the tetrahedral site
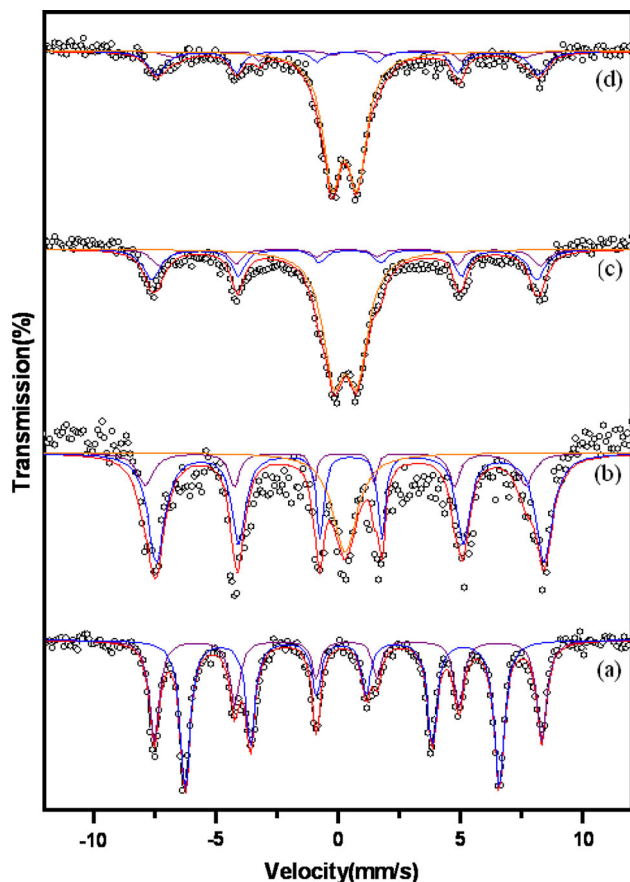
Fig. 6 Mössbauer spectra for (**a**) un-milled (**b**) 3 h (**c**) 6 h and (**d**) 12 h milled samples of YIG at 300 K

completely. Two overlapped sextets include the contribution from Fe^{3+} at the octahedral sites of garnet phase and Fe^{3+} in an octahedral environment' of the orthorhombic orthoferrite phase. These two Fe^{3+}-sites in their respective phases have similar environment as both are surrounded by six oxygen ions. The co-existence of the doublet with the sextets is due to the distribution in particle size and the small particles exhibiting super-paramagnetism at 300 K. This also suggests that the measurement temperature is higher than the blocking temperature of the particles. It is also observed that there is a considerable reduction in the first, second, fifth and sixth line intensity on increasing milling duration, which could be due to the grain boundary magnetic anisotropy in the nano crystalline samples and the spin cluster glass like structure originating from the random interaction of crystalline particles [8].

The observations made from the variation of hyperfine interaction parameters with particle size/milling time (Table 3) may be summarized as follows: (i) Hyperfine field values for YIG and $YFeO_3$ phases decrease. (ii) Isomer shift value for YIG phase increases while Isomer shift values for $YFeO_3$ phase and paramagnetic doublet decrease. (iii) Quadruple shift/splitting show significant but

not systematic variation. (iv) Line widths of YIG and $YFeO_3$ phases are found to increase, while it is found to decrease for paramagnetic doublet. (v) Area ratios for YIG and $YFeO_3$ phases decrease but for paramagnetic doublet area ratio increases with decreasing particle size or increasing milling time.

The reduction in the magnitude of the hyperfine fields on milling is due to the relaxation effects and also because of the surface spins of the small particles. Based on the results of the atomic–scale magnetic modelling of the oxide nanoparticles, Kodama et al. [62] have proposed a model of the spin distribution within nanoscale ferrite particles consisting of ferrimagnetically aligned core spins and a spin glass like surface layer and this surface spin disorder in ferrimagnetic nano-particles is due to broken exchange bonds in the near surface layers. Alternately, the loss of oxygen during milling might have reduced some of the ferric (Fe^{3+}) ions to ferrous (Fe^{2+}) ions giving rise to higher values of the isomer shift and smaller values for the hyperfine fields [20].

3.6. Thermal variation of low field ac susceptibility

The plots of thermal variation of low field (0.5 Oe) ac susceptibility, (χ_{ac}(T)), for un-milled and milled samples of YIG are depicted in Fig. 7(a)–7(d), which exhibit normal ferrimagnetic behaviour. It is observed that all the milled samples show two magnetic transitions. The first transition is relatively sharp and it is in vicinity of the Neel temperature (T_{N1}) of un-milled YIG (~ 557 K), while the second transition is blurred, corresponding to Neel temperature, $T_{N2} = 640$ K of weak ferromagnetic $YFeO_3$ phase [63]. The plots exhibit the tailing effect for temperature $T > T_{N2}$. It is also important to note that transition temperatures and tailing effect decrease with increasing milling time. The breaking of the super-exchange bonds as a result of oxygen vacancies and the defects introduced upon mechanical milling weakens the super-exchange interactions and lower the Neel temperature. The decrease in T_N with the milling time suggests reduction in ferrimagnetic ordering and weakening of magnetic coupling. In other words, the degree of long range ordering decreases as expected due to the presence of large grain boundary volume fraction in the milled samples and as a result Neel temperature is expected to decrease. The tailing effect in the χ_{ac}(T) plots is due to 'spin clusters', which are small groups of atoms with a kind of magnetic short-range order. These clusters of local spin order within a matrix of the spin disorder, which constitutes a paramagnetic phase. The observed decrease in tailing effect with milling time may be due to the increase in micro-structural uniformity in the material.

Table 3 Mossbauer hyperfine interaction parameters at 300 K

Milling time	Hyperfine field (±1 kOe)	Isomer shift (±0.05 mm/s)	Quadrupole shifting (±0.06 mm/s)	line width (±0.05 mm/s)	Relative intensity (±1 %)	Phase (site)
Un-milled	490.2	0.380	0.051	0.429	40.29	YIG (octa.)
	397.3	0.152	0.022	0.443	59.71	YIG (tetra.)
3 h	480.9	0.077	−0.359	0.282	17.95	YIG (octa.)
	490.6	0.516	−0.035	0.360	61.54	YFeO$_3$
	–	0.295	–	1.20	20.51	Singlet
6 h	482.3	0.419	0.120	0.572	13.30	YIG(octa.)
	487.0	0.369	−0.242	0.631	26.02	YFeO$_3$
	–	0.309	0.963	1.05	60.67	Doublet
12 h	441.0	0.699	−0.443	0.620	8.66	YIG(octa.)
	483.7	0.400	0.034	0.626	24.54	YFeO$_3$
	–	0.282	1.02	0.930	66.80	Doublet
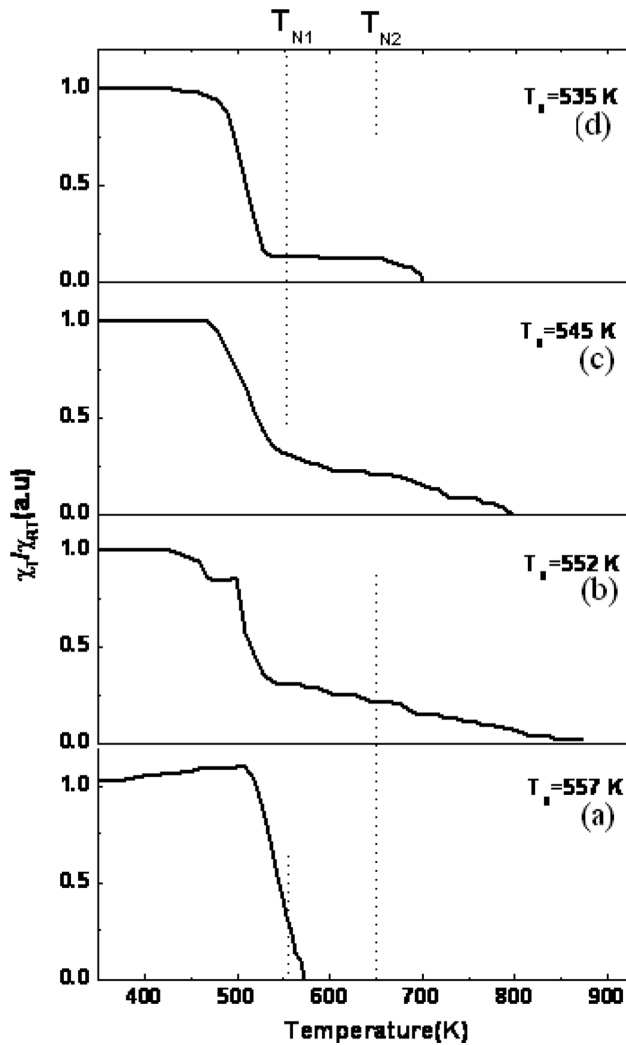
Fig. 7 Temperature dependence of ac susceptibility, χ_T/χ_{RT}, for (**a**) un-milled (**b**) 3 h (**c**) 6 h and (**d**) 12 h milled samples of YIG

The decrease in T_N with particle size for YIG could be explained on the basis of the finite size scaling theory [64]. This theory predicts that the shift in the transition temperature from that of the bulk should depend on a dimension of the system in the following manner:

$$\frac{T_N(\infty) - T_N(D)}{T_N(\infty)} = \left(\frac{D}{D_0}\right)^{\frac{-1}{\varsigma}} \tag{1}$$

where $T_N(D)$ is the Neel temperature as a function of particle size (D), $T_N(\infty)$ is the bulk Neel temperature, D_0 is a constant, it should be of the order of the characteristics microscopic dimension of the system and ς is the critical exponent of the correlation length. Depending on the boundary conditions, geometry and interaction, the change in T_N may be positive or negative. According to Chen et al. [65], it is possible that T_N decreases due to some unknown surface effect. For nano particles a significant fraction of atoms is on the surface and it is reasonable to expect their magnetic interaction to be different hence a different average Neel temperature. Since, the ratio of surface to bulk atoms in a particle is proportional to $1/D$, such an effect, if linearly dependent on the specific surface area, might yield a change in T_N proportional to $1/D$ which would be mathematically equivalent to above Eq. (1) with $\varsigma = 1$.

The straight line in Fig. 8 is obtained as a result of fitting the experimental data using Eq. (1). The parameters obtained from the fit are, $\varsigma = 0.66 \pm 0.03$ and $D_0 = 14.845 \pm 0.01$ Å. This value of ς agrees well with those predicted by the isotropic three-dimensional Heisenberg model [66] which is in the range from $\varsigma = 0.65 \pm 0.07$ to 0.733 ± 0.02. The value of D_0 is of the order of the lattice constant of YIG and hence fulfils its identification on a microscopic length scale. Thus, it is concluded that a finite size scaling describes the shift in T_N well.
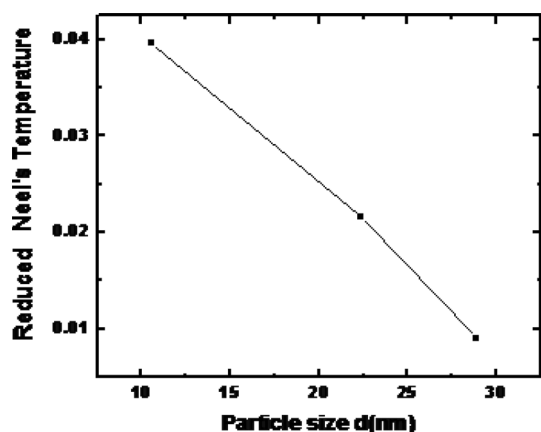
Fig. 8 Reduced Neel's temperature shift versus particle diameter

3.7. High field magnetization studies

Figure 9(a) and 9(b) show magnetization hysteresis curves measured at 20 K for un-milled and 9 h milled samples of $Y_3Fe_5O_{12}$. The saturation magnetization (σ_s) value is found to decrease from 40 emu/g for un-milled sample to 0.3 emu/g for 9 h milled sample, while coercivity (H_c) value is found to increase from 189 Oe for un-milled sample to 590 Oe for 9 h milled sample. According to Greneche et al. [67], the single domain size for the YIG is 300 nm and it is found that for the 200 nm particles, coercivity is maximum. Since, the particle size (13.3 nm, Table 2) of 9 h milled sample is much below the single domain size, the coercivity is expected to decrease with particle size reduction. In contrary to expectation, we have observed 3 times increase in coercivity value for 9 h milled sample compared with coercivity value for un-milled sample. The observed increase in coercivity at 20 K for 9 h milled sample may be due to the increase in the surface anisotropy for smaller particles [20]. Moreover, the observed increase in H_c for 9 h milled sample, may also be due to presence of magnetically hard secondary phase of $YFeO_3$ in the sample. It has been reported that for yttrium orthoferrite, $H_c = 24.6$ kOe at 250 K [49].

The σ_s value is found to reduce by more than two order of magnitude for 9 h milled sample. The much lower value of σ_s could be ascribed to one or more of the following reasons: (i) Upon milling, decomposition process is accelerated and a fraction of iron ions convert into antiferromagnetic $YFeO_3$ which has very low saturation magnetization (1.23 emu/g). Therefore, the total saturation magnetization of the milled sample decreases with milling time. The observed σ_s value (0.3 emu/g) for 9 h milled sample is much lower than the σ_s value for $YFeO_3$. This suggests that beside formation of $YFeO_3$, other factors also contribute to lowering the σ_s value. (ii) The second one is due to defects and strain in the sample induced by ball
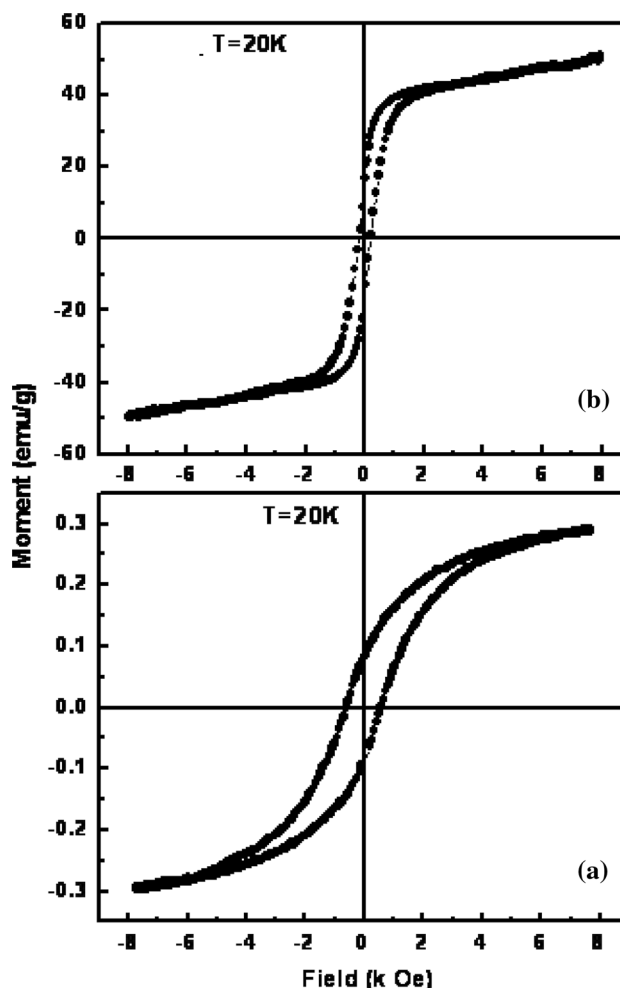

Fig. 9 Magnetization hysteresis curves measured at 20 K for (**a**) 9 h milled and (**b**) un-milled samples of $Y_3Fe_5O_{12}$

milling [68]. (iii) The non-saturation of the loop suggests the presence of the canted spin structure in the milled sample. The canted spin structure could arise due to weakening of the super exchange interaction on mechanical milling, which could cause structural damages and defects. The canted spin structure is linked to the effective anisotropy, which increases because of the lattice strain introduced on milling [20]. (iv) The surface structure disorder also contributes to the spin canting [69].

Further studies on magnetic parameters using dc magnetization measurements have been carried out. Figure 10 shows typical plot of magnetization versus temperature (M–T) recorded in zero-field cooled (ZFC) and field cooled (FC) modes in an external magnetic field of 200 Oe for 9 h milled sample of YIG. The ZFC magnetization is recorded by first cooling the samples from 273 to 20 K in zero magnetic fields, then applying the magnetic field and recording the moment during the warming cycle. FC pattern is recorded by first cooling the sample from 273 K
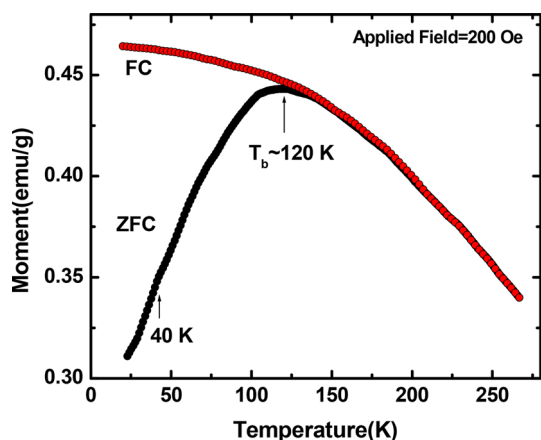
Fig. 10 FC and ZFC magnetization versus temperature curves for 9 h milled sample

down to 4 K in the external magnetic field and then warming it up to 273 K and recording the moment. The ZFC curve indicates that the milled sample exhibits a crystalline size distribution.

In an assembly of crystallites with different particle sizes, the variation of magnetization with temperature arises from the contribution of both ferrimagnetic and super-paramagnetic phases in the milled samples of YIG. The presence of ferrimagnetic phase gives a decrease of magnetization with increasing temperature. Above 20 K, the increase with temperature of ZFC curve can be described to the presence of super-paramagnetic crystallites, which should give a maximum in the ZFC curve [70]. We have observed broad maximum in the temperature range 100–130 K, indicating the blocking of most of the larger crystallites. The ZFC curve shows a shoulder $(T \sim 40 \text{ K})$, indicating the blocking of most of the smaller crystallites. As shown in the Fig. 10, the region of irreversibility disappears for T > 140 K. Thus, the behaviour of the ZFC sample can be explained by the co-existence of both ferrimagnetic and super-paramagnetic phases. The contribution of the super-paramagnetic phase consists of two parts with different blocking temperatures due to crystallite sizes.

4. Conclusions

The high energy ball milling induced structural, infrared spectral, magnetic, electrical and dielectric properties modifications in pristine $Y_3Fe_5O_{12}$ composition have been studied by means of various experimental techniques. The important results are as under: the un-milled sample possesses single phase *bcc* structure, on milling; $Y_3Fe_5O_{12}$ decomposes into $Y_3Fe_5O_{12}$ and $YFeO_3$ phases. The lattice constant value for garnet phase is found to change, while

that of orthoferrite phase remains unaffected with milling. The average particle size is found to decrease while average lattice strain, surface area and surface free energy are found to increase with milling duration. The milled samples of $Y_3Fe_5O_{12}$ show two characteristic absorption bands: high frequency absorption band is due to combine effect of asymmetric stretching vibrations of the tetrahedron of YIG-phase and the motion of in-plane oxygen atoms of $YFeO_3$-phase, while low frequency absorption band involves bending motion of tetrahedron of YIG phase and apical oxygen vibrations of $YFeO_3$.SEM and TEM image analyses reveal considerable changes in particle size, shape and size distribution with milling duration. ^{57}Fe Mössbauer spectral analysis shows presence of paramagnetic singlet/doublet for milled samples due to the distribution in particle size and the super-paramagnetism exhibited by small particles at 300 K. The reduction in the magnitude of the hyperfine fields on milling is due to the relaxation effects and also because of the surface spins of the small particles. The hyperfine parameters show remarkable change with milling. The Mossbauer studies give an indication for the loss of oxygen on milling. Temperature dependence of ac susceptibility curve for the milled samples shows two magnetic transitions, one due to ferrimagnetic YIG-phase and another due to weak ferromagnetic $YFeO_3$ phase. The shift in Neel temperature with particle size reduction can be described by finite size scaling. The observed increase in coercivity and decrease in saturation magnetization for 9 h milled sample are mainly due to strain induced increase in surface anisotropy on milling.

Not only the particle size but also mechanical milling induced strain should be given due consideration during the preparation of nano structured garnets, since it is shown to greatly influence the phase formation and physical properties.

References

[1] S Yu-Jhan, Q Xiaoding, L Chun-Rong and H J Chun-Andrew *J. Appl. Phys.* **109** 07A508 (2011)

[2] M R Mahmood, T Soga, M H Mamat, Z Khusaimi and A M Nor *Adv. Mater. Res.* **667** 10 (2013)

[3] V V Abramova, A Slesarev and A Sinitskii *J. Mater. Chem. C.* **1** 2975 (2013)

[4] F Studer, C Houpert, D Groult and M Toulemonde *Rad. Eff. Def. Solids* **110** 55 (1989)

[5] T Takanori, K Teruhiro and H Kenichi *J. Appl. Phys.* **110** 053909 (2011)

[6] T Chien-Yie, L Chung-Kwei, C Hua-Chi, L Kuo-Shung and L I Nan *Mater. Chem. Phys.* **105** 408 (2007)

[7] H Donnerberg and C R A Catlow *J. Phys. Condens. Matter* **5** 2947 (1993)

[8] D Prabhu, A Narayanasamy, K Shinoda, B Jeyadeven, J M Greneche and K Chattopadhyay *J. Appl. Phys.* **109** 013532 (2011)

[9] C S Pathak, D D Mishra, V Agarawala and M K Mandal *Indian J. Phys.* **86** 777 (2012)

[10] R S Pandi, R Chokkalingam and M Mahendran *Indian J. Phys.* **86** 787 (2012)

[11] C C Koch *Nano Struct. Mater.* **9** 13 (1997)

[12] T Ramesh, S R Murty and R S Shinde *Integr. Ferroelectr.* **118** 67 (2010)

[13] B A Gizhevskii et al. *Phys. Solid State* **51** 1836 (2009)

[14] Y Hongtao, L Zeng, C Lu, W Zhang and X Guangliang *Mater. Character* **62** 378 (2011)

[15] S Hosseini Vajargah, H R Madaah Hosseini and Z A Nemati *J. Alloys Comp.* **430** 339 (2007)

[16] B Raneesh, I Rejeena, P U Rehana, P Radhakrishnan, A Saha and N Kalarikkai *Ceram. Int.* **38** 1823 (2012)

[17] T Gaudisson et al. *J. Am. Ceram. Soc.* **96** 3094 (2013)

[18] N Yahya and P Puspitasari *J. Nano Res.* **21** 131 (2013)

[19] H M Widatallah et al. *ICAME-2007* **183** 259 (2009)

[20] R J Joseyphus, A Narayanasamy, A K Nigam and R J Krishnan *J. Magn. Magn. Mater.* **296** 57 (2006)

[21] R J Joseyphus et al. *J. Magn. Magn. Mater.* **272–276** 2257 (2004)

[22] M Ristic, I Nowik, S Popovic, I Felner and S Music *Mater. Lett.* **57** 2584 (2003)

[23] F S Jesus, C A Cortes, R Valenzuela, S Ammar and A M Bolarin-Miro *Ceram. Int.* **38** 5257 (2012)

[24] C A Cortes-Escobedo et al. *Adv. Mater. Phys. Chem.* **3** 41 (2013)

[25] Y Jun Wu, C Yu, X Ming Chen and J Li *J. Am. Ceram. Soc.* **95** 1671 (2012)

[26] W Xu, J Yang, Y Jin and T Qiu *J. Euro. Ceram. Soc.* **33** 1023 (2013)

[27] P U Sharma and K B Modi *Phys. Scr.* **81** 015601 (2010)

[28] P U Sharma, K B Modi, V K Lakhani, K B Zankat and H H Joshi *Ceram. Int.* **33** 1543 (2007)

[29] P U Sharma, S N Dolia, R Kumar and K B Modi *Radi. Effe. Def. Solid* **166** 648 (2011)

[30] P U Sharma, M K Roy, Ravi Kumar, H C Verma, H H Joshi and K B Modi *Hyper. Inter.* **187** 117 (2008)

[31] K B Modi and P U Sharma *Rad. Eff. Def. Solids* **169** 723 (2014)

[32] K B Modi and P U Sharma *Rad. Eff. Def. Solids* **168** 967 (2013)

[33] K B Modi and P U Sharma *Phys. Scr.* **88** 025702 (2013)

[34] N H Vasoya et al. *Ceram. Int.* **36** 947 (2010)

[35] K B Modi, T K Pathak, N H Vasoya, V K Lakhani, G J Baldha and P K Jha *Indian J. Phys.* **85** 411 (2011)

[36] K B Modi, S J Shah, N B Pujara, T K Pathak, N H Vasoya and I G Jhala *J. Mol. Struct.* **1049** 250 (2013)

[37] C Suryanarayana *Prog. Mater. Sci.* **46** 1 (2001)

[38] E J J Mallmann, A S B Sombra, J C Goes and P B A Fechine *Solid State Pheno.* **202** 65 (2013)

[39] C R K Murthy, S D Likhite and P Sashrabudhee *Proc. Indian Acad. Sci.* **87A** 245 (1978)

[40] C Dong *J. Appl. Cryst.* **32** 838 (**1999**)

[41] A Beiravand, M Mehdipour, Y A Amighian and M Mozaffari *Life Sci. J.* **10** 155 (2013)

[42] P Ayyub, V R Palker, S Chattopadhyay and M Multani *Phys. Rev. B* **51** 6135 (1995)

[43] H G Drickamer *Solid State Physics: Advances in Research and Application,* vol 17, ed. by F Seitz, D Turnbull (New York: Academic Press Inc.) p 1 (1965)

[44] S D Shenoy, P A Joy and M R Anantharaman *J. Magn. Magn. Mater.* **269** 217 (2004)

[45] N Rezlescu, E Rezlescu, C Pasnicu and M L Craus *J. Phys. Condens. Matter* **6** 5707 (1994)

[46] X Chao, Z Yang, M Dong and Y Zhang *J. Magn. Magn. Mater.* **323** 2012 (2011)

[47] A R Stokes and A J C Wilson *Proc. Phys. Soc.* **56** 174 (1994)

[48] G Mathew, J Asha Mary, S S Nair, P A Joy and M R Anantharaman *J. Magn. Magn. Mater.* **302** 190 (2006)

[49] E Ryshkewitch. *Oxide Ceramics, Physics Chemistry and Technology* (New York: Academic Press Inc.) (1960)

[50] A M Hofmeister and K R Campbell *J. Appl. Phys.* **72** 638 (1992)

[51] S Mathur et al. *Chem. Mater.* **16** 1906 (2004)

[52] S Venugopalan, M Dutta, A R Ramdas and J P Remeika *Phys. Rev. B* **31** 1490 (1985)

[53] G V SubbaRao, C N R Rao and J R Ferraro *Appl. Spectr.* **24** 436 (1970)

[54] I Fedorov et al. *Phys. Rev. B* **60** 11875 (1999)

[55] N Sivakumar, A Narayanasamy, N Ponpandian and G Govindaraj *J. Appl. Phys.* **101** 084116 (2007)

[56] C Upadhyay *PhD Thesis* IIT-Kanpur p 40 (2003)

[57] R Bauminger, S G Cohen, A Marinov, S Ofer and E Segal *Phys. Rev.* **122** 1447 (1961)

[58] S Ho Lee, K P Chae, S W Hong and Y B Lee *Solid State Commun.* **83** 97 (1992)

[59] Y B Lee, K P Chae and S H Lee *J. Phys. Chem. Solids* **62** 1335 (2001)

[60] J M Constantini, J P Salvetat and F Brisard *J. Appl. Phys.* **82** 5063 (1997)

[61] F Studer, C Houpert, M Toulemonde and E Dartyge *J. Solid State Chem.* **91** 238 (1991)

[62] R H Kodama, A E Berkowitz, E J McNiff and S Foner *J. Appl. Phys.* **81** 5552 (1997)

[63] M Eibschutz, S Shtrikman and D Treves *Phys. Rev.* **156** 562 (1967)

[64] M N Barber *Phase Transitions and Critical Phenomena*, vol 8 (ed.) C Domb and J L Lebowitz (New York: Academic Press Inc.) p 145 (1983)

[65] J P Chen, C M Sorensen, K J Klabunde, G C Hadjipanayis, E Devlin and A Kostikas *Phys. Rev. B* **54** 9288 (1996)

[66] S N Kaul *J. Magn. Magn. Mater.* **53** 5 (1985)

[67] P Vaqueiro, M A Lopez-Quintela, J Rivas and J M Greneche *J. Magn. Magn. Mater.* **169** 56 (1997)

[68] J S Jiang, L Gao, X L Yang, J K Guo and H L Shen *J. Mater. Sci. Lett.* **18** 1781 (1999)

[69] G F Goya, H R Rechenberg and J Z Jiang *J. Appl. Phys.* **84** 1101 (1998)

[70] S C Yu, Y Y Song, L F Kiss and I Vincze *J. Magn. Magn. Mater.* **203** 316 (1999)